Multireference CI Study of Excitation Energies and Potential Energy Surfaces of CH_3F[†]

Glauco F. Bauerfeldt* and Hans Lischka*

Institute for Theoretical Chemistry and Molecular Biology, University of Vienna, Währingerstrasse 17, A-1090 Vienna, Austria

Received: October 13, 2003; In Final Form: December 2, 2003

Vertical excitation energies for the eight singlet-excited electronic states 1^1E ($2e \rightarrow 3s$), 2^1E ($2e \rightarrow 3p_{a1}$), 3^1E ($2e \rightarrow 3p_e$), 2^1A_1 ($2e \rightarrow 3p_e$), 1^1A_2 ($2e \rightarrow 3p_e$), 3^1A_1 ($2p_{a1} \rightarrow 3s$), 4^1A_1 ($2p_{a1} \rightarrow 3p_{a1}$), and 4^1E ($2p_{a1} \rightarrow 3p_e$) of CH_3F were investigated using the SA-MCSCF, MR-CISD, and MRCISD+Q approaches. Our results mostly confirm the experimental assignments but suggest some modifications for the main contribution to the maximum observed in the range from 12.5−14 eV. The dissociation channels for the production of fluorine atoms have been characterized. Potential energy curves for the dissociation of the CF bond under C_{3v} symmetry restrictions were computed for all states mentioned above leading to the ground-state dissociation channel $CH_3(\tilde{X}^2A_2'') + F(^2P)$, the excited-state channels $CH_3(3s\ ^2A_1') + F(^2P)$ and $CH_3(3p\ ^2A_2'') + F(^2P)$ and also to the ionic limit $CH_3^+(^1A_1') + F^-(^1S)$. All curves except the one for the ionic state show repulsive behavior. The search for a global minimum for the ionic state led to the structure $H_2CH^+F^-$ in the $3^1A'$ state. It is strongly bound by 5.67 eV with respect to the ionic dissociation limit of $F^- + CH_3^+$.

I. Introduction

Much effort has been spent on the understanding of physical−chemical properties as well as dissociation profiles of fluorinated hydrocarbons because of their role in plasma etching and related processes used in microelectronics manufacturing.[1] In reactive ion etching, either plasma or laser-induced, the most important reaction is the formation of fluorine atoms,[2−5] which further react with silicon or any other semiconductor material promoting the etching. Methyl fluoride is a prototype fluorinated hydrocarbon for which the fundamental spectroscopic properties and dissociation paths can be studied in detail. Jalbout[6] has calculated ionization potentials as well as ground-state dissociation energies for several H-atom dissociation channels of CH_3F and CH_3Cl. Espinosa-Garcia[7] has studied the enthalpy of formation of CH_3F using Møller−Plesset fourth-order perturbation theory (MP4), quadratic configuration interactions (QCISD), and coupled cluster (CC) methods with extended basis sets. Finally, halogen−carbon bond-dissociation energies have been determined at the MP2 and CCSD(T) levels.[8]

The structure of CH_3F in the electronic ground state has been determined by Duncan[9] and reevaluated by Egawa,[10] who combined electron diffraction data with ground-state rotational constants to obtain accurate geometrical parameters. CCSD(T) calculations yielded geometries[11] in good agreement with those found by Egawa.[10] Recently, the vacuum UV photoabsorption spectrum of CH_3F has been described in detail in the range from 7 to 24 eV, showing broad and structureless bands assigned as transitions to Rydberg states.[12]

Although a great amount of work has been done, to the best of our knowledge no theoretical investigations dedicated to the understanding of the potential energy surfaces of CH_3F and to the connection between vertical excitations and CF dissociation channels are available. Therefore, in this work a detailed theoretical study of the dissociation of the CF bond in CH_3F has been performed for the ground state as well as for several excited states. To allow a general treatment of excited-state energy surfaces, an extended multireference configuration interaction with singles and doubles (MR-CISD)[13] method has been used. In important cases, full geometry optimizations have been performed using recently developed analytical MR-CI energy gradient methods.[14−16] A total of nine electronic states (including valence and 3s and 3p Rydberg states) have been characterized at multiconfiguration self-consistent field (MCSCF) and MR-CISD levels, including vertical excitations as well as dissociation curves in excited states as a function of the CF distance. From our results, we could confirm spectroscopic assignments of the electronic spectra and reinterpret certain features. Under C_{3v} symmetry restrictions, an energy minimum for an ionic complex ($CH_3^+F^-$) was found in the 2^1A_1 excited state, which actually turned out to be a saddle point of second order. To study the stability of this ionic structure in more detail, bending curves in C_s symmetry along the FCH angle have also been computed, leading to isomeric structures of methyl fluoride that were characterized by full geometry optimizations.

II. MO Scheme, Electronic States, and Structures

The MO scheme for the ground state is given in C_{3v} symmetry by $(1a_1)^2\ (2a_1)^2\ (3a_1)^2\ (4a_1)^2\ (1e)^4\ (5a_1)^2\ (2e)^4$. Orbitals $1a_1$ and $2a_1$ are the core orbitals, and $3a_1$ corresponds to fluorine 2s. Orbitals $4a_1$ and 1e represent the σ_{CH} bonds. Orbital $5a_1$ describes the σ_{CF} bond, and the 2e orbitals are fluorine lone pairs. In addition to these closed-shell valence orbitals, the $6a_1$ orbital, which corresponds to the σ^*_{CF} orbital, was used for the proper description of the dissociation of the CF bond. Orbitals $7a_1$, $8a_1$, and 3e correspond to the 3s, $3p_{a1}$ ($3p_z$), and $3p_e$ ($3p_x$ and $3p_y$) Rydberg orbitals, respectively. The CH_3F molecule was oriented with the CF bond in the direction of the *z* axis.

Calculations on vertical excitations were performed at the MCSCF and MR-CISD levels. State averaging was performed at the MCSCF level, including the ground state and the excited

[†] Part of the special issue "Fritz Schaefer Festschrift".

* To whom correspondence should be addressed. E-mail: glauco.favilla.bauerfeldt@univie.ac.at; hans.lischka@univie.ac.at.

10.1021/jp037091h CCC: $27.50 © 2004 American Chemical Society
Published on Web 03/09/2004

states of interest with equal weight. Definitions for the MCSCF reference wave functions will be given in the next section. In the MR-CISD calculations, the extended Davidson correction[17,18] (MR-CISD+Q) was used for an a posteriori computation of size-extensivity effects. Geometry optimizations were performed at the MCSCF and MR-CISD levels.

Three series of calculations on excited states of CH_3F were performed. In the first set, the vertical excitations from the ground state 1^1A_1 to the Rydberg states 1^1E ($2e \rightarrow 3s$), 2^1E ($2e \rightarrow 3p_{a1}$), 3^1E ($2e \rightarrow 3p_e$), 2^1A_1 ($2e \rightarrow 3p_e$), 1^1A_2 ($2e \rightarrow 3p_e$), 3^1A_1 ($5a_1 \rightarrow 3s$), 4^1A_1 ($5a_1 \rightarrow 3p_{a1}$), and 4^1E ($5a_1 \rightarrow 3p_e$) were investigated. CF dissociation curves for all nine of these electronic states with the remaining geometry parameters fixed were computed. An ionic channel was found for the 2^1A_1 state, and its potential curve showed a minimum under C_{3v} symmetry restrictions corresponding to an ionic complex $CH_3^+F^-$. To search for the true minimum-energy structure of the ionic state, in the second set of calculations a detailed investigation of the CF dissociation profile of the 2^1A_1 state and the 1^1A_1 and 1^1E below was performed. The symmetry-restricted minimum for the ionic complex $CH_3^+F^-$ was characterized as a second-order saddle point in the full coordinate space by vibrational frequency calculations. Following the modes corresponding to these imaginary frequencies by moving the F atom off of the C_3 axis finally resulted in two structures H_2CHF and FH_2CH for the ionic state. By analogy to the C_{3v} case, the orbital schemes for these ionic states in C_s symmetry notation are $1-8a'$ and $1-2a''$. For these structures, geometry optimizations and vibrational frequency calculations were performed. CF dissociation curves for the H_2CHF structure were computed also.

III. Computational Procedures

For the computation of vertical excitations and of dissociation curves for the first nine singlet electronic states of CH_3F, a complete active space (CAS) of six electrons in four orbitals ($5a_1$, 2e, and $6a_1$) was used, augmented by four auxiliary orbitals ($7a_1$, $8a_1$, and 3e), to describe the Rydberg orbitals. This reference space is denoted by CAS(6,4)/AUX(4). These orbitals were selected to take into account the correct dissociation of the CF bond (see below) and to include Rydberg excitations. Only single excitations from the CAS to the AUX space were allowed in the construction of reference spaces. This procedure has already been used successfully for the description of Rydberg states of formaldehyde[19] and butadiene.[20] The cc-pVDZ basis set[21] was employed, augmented with s functions for hydrogen atoms and s, p, and d functions for non-hydrogen atoms[22] and doubly augmented with s and p functions for non-hydrogen atoms[23,24] for the description of the Rydberg orbitals. This basis set will be denoted d-aug′-cc-pVDZ hereafter. The CAS(6,4)/AUX(4) space was used in state-averaged SA-MCSCF calculations and as a reference space in subsequent MR-CISD calculations. Single and double excitations from all reference-occupied orbitals into all virtual orbitals were constructed from all reference configurations to give the space of configuration state functions (CSFs) in the MR-CISD calculation. Only those reference configurations having the symmetry of the state to be calculated were selected. Moreover, the interacting space restriction[25] was applied. The 1s core orbitals were kept frozen. Because in the MCSCF and MR-CISD calculations only Abelian groups could be used, the actual calculations were performed in C_s symmetry. The degeneracy of the orbitals was achieved by appropriate state averaging at the MCSCF level and was controlled throughout the calculations by an inspection of natural orbital (NO) occupation numbers. The experimental geometry[10] ($R_{CF} = 1.383$ Å, $R_{CH} = 1.086$ Å, $\angle_{HCH} = 110.2°$, $\angle_{HCF} = 108.8°$) was used for the computation of vertical excitations. The potential curves for the 1^1A_1, 2^1A_1, and 1^1E states were investigated in more detail using SA-CASSCF(6,4) calculations. Because these states show valence character, double augmentation was not necessary for these calculations. The aug-cc-pVDZ [21,22] basis set and the cc-pVTZ basis set[21] augmented with s and p functions for the hydrogen atoms and s, p, and d functions for non-hydrogen atoms[22] (denoted aug′-cc-pVTZ) were used. MR-CISD calculations were performed on the basis of the CAS-(6,4) reference space.

For the determination of the dissociation limits for the ground state and excited states, three different approaches (cases I−III) were chosen using different choices for CH_3 geometries. In case I, vertical excitations using the optimized CH_3 ground-state geometry were performed. Case II corresponded to adiabatic excitation/ionization in CH_3. In case III, the frozen CH_3 geometry of CH_3F was used. In most cases (see below), the properties of the dissociation products CH_3 and F were computed in the form of a $CH_3 + F$ supermolecule with a C−F distance of 10 Å. For the ionic complex ($CH_3^+F^-$), a C−F distance of 50 Å was chosen, and the remaining ionic interaction was computed as the Coulomb $^1/_R$ energy. In case I, a $CH_3 + F$ supermolecule optimization was performed for the ground state at the MR-CISD level using the CAS(6,4)/AUX(4) reference space and the d-aug′-cc-pVDZ basis set. The dissociation energies were computed as the energy differences between the vertically excited states of the $CH_3 + F$ supermolecule and the ground-state minimum. In case II, the dissociation energies for the excited states were calculated from the ground-state dissociation energy obtained from case I, the adiabatic excitation and ionization energies of CH_3, and the electron affinity of F. In case III, the dissociation energies were directly computed as the asymptotic limit of the dissociation curves where the geometry of CH_3F (except for the CF bond distance) had been kept fixed at the ground-state value.

To compute the adiabatic excitation energies needed for case II and for comparison reasons with the frozen geometry computations of case III, active spaces were selected for the fragments consistent with that for the $CH_3 + F$ supermolecule calculation. For CH_3, this led to an open-shell single-reference configuration with one electron in one orbital (CAS(1,1)) and single excitations into the Rydberg 3s, $3p_x$, $3p_y$, and $3p_z$ orbitals of the auxiliary space, denoted as CAS(1,1)/AUX(4)/d-aug′-cc-pVDZ. For the calculation of the electron affinity of fluorine, the CAS(5,3) and CAS(6,3) (closed-shell) reference spaces were chosen for the fluorine atom and fluoride anion, respectively. For consistency with the previous calculations, the d-aug-cc-pVDZ basis was employed. SA-MCSCF calculations in the CAS(1,1)/AUX(4) and CAS(5,3) spaces, respectively, were performed, followed by MR-CISD/MR-CISD+Q calculations using as a reference space the same space that was used in the MCSCF calculations. Vertical and adiabatic excitation energies were calculated. It is clear that for more accurate calculations on the fragments larger reference spaces and basis sets could have been selected. The main purpose of the results presented here is the assessment of the accuracy of the methods used for the calculation of the entire potential energy curves.

The bending potential energy curves in the FCH angle were constructed for the four low-lying singlet electronic states $1^1A'$, $2^1A'$, $1^1A''$, and $3^1A'$. These bending curves connect three different CH_3F structures (Figure 1): the C_{3v} structure $CH_3^+F^-$, in which $\angle_{FCH'}$ is 90°, and the bent H_2CHF and FH_2CH structures. In the H_2CHF structure, the fluorine atom is located

TABLE 1: Vertical Excitation Energies (eV) Calculated at the MCSCF, MR-CISD, and MR-CISD+Q Levels Using the d-aug′-cc-pVDZ Basis Set in Comparison to Experimental Results[a]

				vertical excitation energies			
state	assignment	$f(\times 10^{-3})$	$\langle r^2\rangle$	MCSCF	CISD	CI+Q	exptl[b]
E_{tot}[c]				−139.018668	−139.402448	−139.446222	
1^1E	$2e \rightarrow 3s$	1.1	59.15	7.88	9.48	9.67	9.37
2^1E	$2e \rightarrow 3p_{a1}$	25.7	73.85	8.44	9.98	10.06	10.04
3^1E	$2e \rightarrow 3p_e$	9.5	88.13	8.85	10.61	10.83	11.27
2^1A_1	$2e \rightarrow 3p_e$	30.4	88.27	8.85	10.61	10.85	
1^1A_2	$2e \rightarrow 3p_e$	0.0	88.83	8.88	10.66	10.89	
3^1A_1	$2p_{a1} \rightarrow 3s$	12.3	60.96	11.59	13.37	13.76	13.57
4^1A_1	$2p_{a1} \rightarrow 3p_{a1}$	203.1	77.17	12.20	13.88	14.18	
4^1E	$2p_{a1} \rightarrow 3p_e$	14.5	87.32	12.47	14.35	14.69	

[a] Oscillator strengths f and $\langle r^2\rangle$ expectation values (in au) calculated at the MR-CISD level are included. [b] Reference 12. [c] Ground-state energy in hartrees.

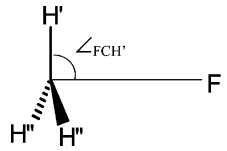

Figure 1. CH_3F structure and definition of the FCH′ angle.

opposite to the CH′ bond ($\angle_{FCH'}$ is 0°), and in FH_2CH, the fluorine atom is positioned in front of the CH''_2 group ($\angle_{FCH'}$ is 180°). C_s symmetry is maintained with the symmetry plane bisecting the CH''_2 group and containing the F atom. The calculations for the bending curves were performed at the MR-CISD level using a CAS(12,7) reference space containing the 4−8a′ and 1−2a″ valence orbitals and the aug-cc-pVDZ basis set. This larger active space takes into account the reordering of active and doubly occupied orbitals along the bending potential curve. Full geometry optimizations were performed for the $CH_3^+F^-$, H_2CHF, and FH_2CH structures of the ionic $3^1A'$ state at the MR-CISD level using the CAS(6,4) reference space containing the 6−8a′ and 2a″ orbitals and the aug-cc-pVDZ and aug′-cc-pVTZ basis sets. A vibrational analysis was performed at the SA-CASSCF level to characterize the stationary points.

The calculations have been carried out using the COLUMBUS quantum chemical program package.[26−29] The atomic orbital and atomic orbital derivative integrals have been computed with program modules taken from DALTON.[30] Geometry optimizations were performed in natural internal coordinates[31] using the GDIIS procedure.[32] Force constants were computed by finite differences in energy gradients, and the harmonic vibrational frequencies were computed by the program SUSCAL.[33]

IV. Results and Discussion

A. Vertical Excitation Energies. A total of nine singlet electronic states, including the ground state, were calculated, namely, 1^1A_1, 1^1E, 2^1E, 3^1E, 2^1A_1, 1^1A_2, 3^1A_1, 4^1A1, and 4^1E. Vertical excitation energies calculated at the SA-CAS(6,4)/AUX(4), MR-CISD, and MR-CISD+Q levels using the d-aug′-cc-pVDZ basis set are shown in Table 1 in comparison with available experimental results.[12] Oscillator strengths f and expectation values $\langle r^2\rangle$ computed at the MR-CISD level are tabulated also. From the data given in this table, one can note that the MCSCF results are always considerably lower than the MR-CISD values, whereas the MR-CISD and MR-CISD+Q values are found to be in good agreement with the experimental data, as will be discussed below.

The 1^1E singlet state is characterized by an excitation from the 2e orbitals to the Rydberg 3s orbital. The vertical excitation energy determined for the $1^1A_1 \rightarrow 1^1E$ transition is 9.48 eV at the MR-CISD level and 9.67 eV at the MR-CISD+Q level (Table 1), results that are in good agreement with the experimental value.[12] A single excitation from the 2e orbitals to the Rydberg $3p_{a1}$ orbital generates state 2^1E with vertical excitation energies of 9.98 and 10.06 eV at the MR-CISD and MR-CISD+Q levels, respectively. The latter is in perfect agreement with the experimental value of 10.04 eV.[12] An excitation from 2e to the Rydberg $3p_e$ orbitals generates states 3^1E, 2^1A_1, and 1^1A_2. Calculated excitation energies are in the range of 10.61−10.67 eV at the MR-CISD level and 10.83−10.89 eV at the MR-CISD+Q level. The range of the experimental band assigned as a $2e \rightarrow 3p$ transition is between 10.8 and 11.8 eV and has a band maximum at 11.27 eV.[12] Alternatively, this band maximum has also been assigned to a $2e \rightarrow 4s/3d$ transition.[34,35] From our MR-CISD+Q calculations, one can see that the $2e \rightarrow 3p$ transitions are located more than 0.3 eV below the experimental band maximum of 11.27 eV, a fact that leads us to support the assignment of the band maximum to a $2e \rightarrow 4s/3d$ transition. Because our active space did not include higher Rydberg orbitals such as 4s and 3d, these assignments could not be confirmed explicitly.

States 3^1A_1, 4^1A_1, and 4^1E are generated by single excitations from the σ_{CF} ($5a_1$) orbital to Rydberg orbitals 3s, $3p_{a1}$, and $3p_e$, respectively. At the MR-CISD+Q level, the vertical excitation energies for the $3\ ^1A_1$, $4\ ^1A_1$, and $4\ ^1E$ states are 13.76, 14.18, and 14.69 eV, respectively. The band maximum of the photoabsorption spectrum assigned as a $\sigma_{CF} \rightarrow 3s$ excitation is located at 13.57 eV.[12] Table 1 shows that the calculated oscillator strength for the $\sigma_{CF} \rightarrow 3s$ transition is smaller by more than 1 order of magnitude than the one for the $\sigma_{CF} \rightarrow 3p_{a1}$ excitation. Although the maximum value observed in ref 12 agrees well with our calculated value for the $\sigma_{CF} \rightarrow 3s$ excitation, the calculated intensities show that the main contribution to this band comes from the $\sigma_{CF} \rightarrow 3p_{a1}$ excitation rather than from $\sigma_{CF} \rightarrow 3s$. Excitations in the range of 11.8−13.2 eV assigned as $2e \rightarrow 6s/5d$[12] have also been reported. However, these excitations were not taken into account in our calculations.

B. C_{3v} Potential Energy Curves and Dissociation Paths. Potential energy curves for the CF bond dissociation were calculated for all states investigated in the previous section, keeping the CH_3 geometry frozen at the experimental geometry of the ground state. Figure 2 shows the dissociation curves calculated at the MR-CISD+Q level. A detailed picture in the range of 1.2 to 2.4 Å shows the changes in configurations (Figure 3). The ground-state curve shows a typical dissociation profile of a bound molecule. For small displacements of the CF distance, the total wave function is mainly of closed-shell character. As the CF distance increases, the weight of the single excitation from the σ_{CF} to the $7a_1$ orbital increases. The latter

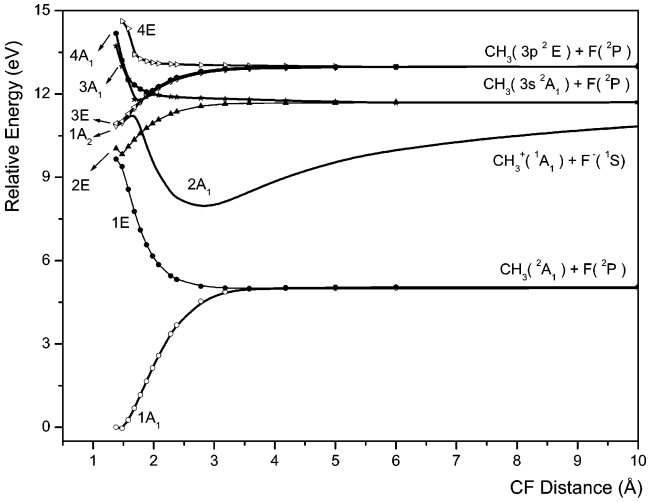

Figure 2. Dissociation curves for CH_3F calculated at the MR-CISD+Q level using a CAS(6,4)/AUX(4) reference space and the d-aug′-cc-pVDZ basis set.

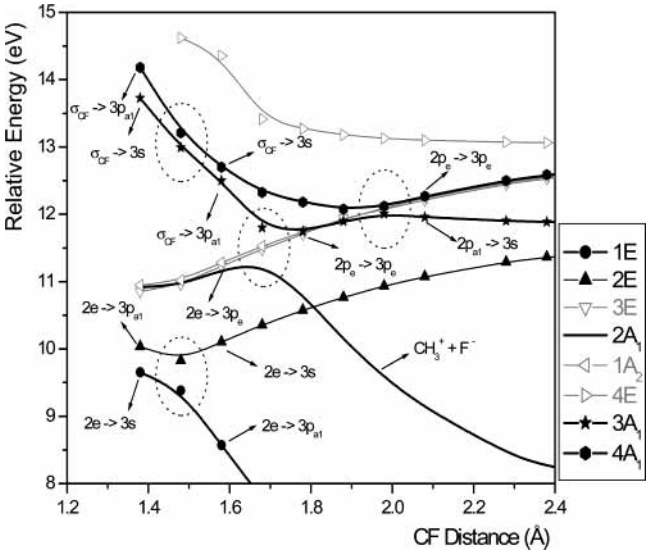

Figure 3. Main configurations and avoided crossings in the dissociation curves for CH_3F calculated at the MR-CISD+Q level using a CAS-(6,4)/AUX(4) reference space and the d-aug′-cc-pVDZ basis set.

smoothly changes from Rydberg 3s character to a $C(p_{a1})$ orbital, and the σ_{CF} orbital is transformed to $F(p_{a1})$ so that for larger CF distances the dominant configuration $F(p_{a1})^1C(p_{a1})^1$ is obtained. The remaining orbitals resemble well the isolated F and CH_3 orbitals. The $6a_1$ orbital changes from σ^*_{CF} character to a virtual orbital on fluorine.

The 1^1E and 2^1E states are vertically assigned to excitations $2e \rightarrow 3s$ and $2e \rightarrow 3p_{a1}$, respectively. However, as soon as the CF distance is stretched by 0.1 Å, an avoided crossing between these states is found with a concomitant change in the electronic configuration (Figure 3). The 1^1E curve is now characterized by the configuration $2e^13p_{a1}^1$, and the 2^1E curve is characterized by the configuration $2e^13s^1$. The Rydberg $3p_{a1}$ orbital changes character along the dissociation curve to become the atomic $C(p_{a1})$ orbital, and the 2e orbitals transform into the atomic $F(p_e)$ orbitals. At larger displacements, the dominant configuration of the 1^1E curve is characterized by the single occupancy of one of the $F(p_e)$ orbitals (the other one is doubly occupied) and the $C(p_{a1})$ orbital. This is equivalent to the configuration found for the ground-state dissociation because at the dissociation limit the $F(p_{a1})$ and $F(p_e)$ orbitals are degenerate.

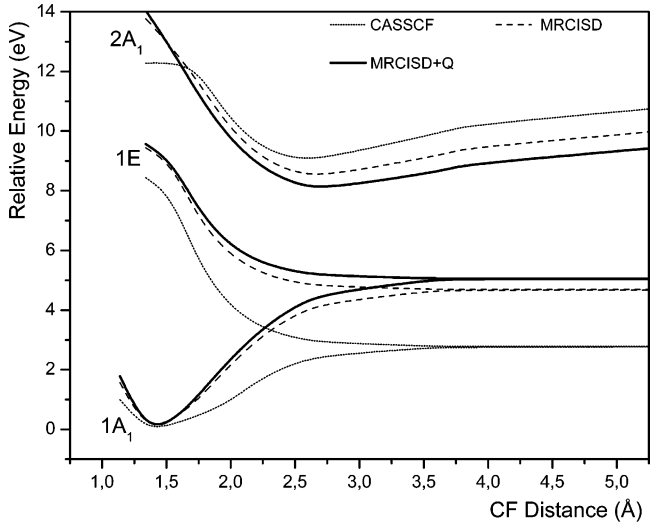

Figure 4. Dissociation curves for CH_3F calculated at the CASSCF, MR-CISD, and MR-CISD+Q levels using a CAS(6,4) reference space and the aug′-cc-pVTZ basis set.

Several avoided crossings can be found between the 2^1A_1, 3^1A_1, and 4^1A_1 states in Figure 3. The first avoided crossing occurs at about 1.5 Å between the 3^1A_1 and 4^1A_1 states, which initially correspond to $\sigma_{CF} \rightarrow 3s$ and $\sigma_{CF} \rightarrow 3p_{a1}$ excitations, respectively. At 1.7 Å, another avoided crossing can be found between states 2^1A_1 and 3^1A_1. After passing this avoided crossing in the direction toward larger CF bond distances, the dominant configurations found for these two states are $\sigma_{CF} \rightarrow 3p_{a1}$ (2^1A_1) and $2p_e \rightarrow 3p_e$ (3^1A_1). At 2 Å, an avoided crossing between states 3^1A_1 and 4^1A_1 is found such that they assume at larger distances the configurations $2p_{a1} \rightarrow 3s$ and $2p_e \rightarrow 3p_e$, respectively. It is also interesting to point out the broad avoided crossing found between the 1^1A_1 and 2^1A_1 states. At smaller CF distances, state 1^1A_1 has a dominant closed-shell configuration ($(\sigma_{CF})^2(3p_{a1})^0$), whereas a covalent configuration ($(\sigma_{CF})^1(3p_{a1})^1$) is found for state 2^1A_1. After the avoided crossing, state 2^1A_1 has closed-shell, ionic character, and state 1^1A_1 assumes covalent character, which finally leads to the correct dissociation behavior. The 2^1A_1 state shows a broad minimum typical of an ionic interaction. Not shown in the figures is a final avoided crossing between states 2^1A_1 and 3^1A_1 found at about 20 Å. The three states $2-4^1A_1$ finally go asymptotically to $CH_3(3s\ ^2A_1) + F\ (^2P)\ (2^1A_1)$, $F^-(^1S) + CH_3^+\ (^1A_1)\ (3^1A_1)$, and $CH_3(3p\ ^2E) + F\ (^2P)\ (4^1A_1)$, respectively.

The asymptotic limit for the dissociation of the 3^1E, 1^1A_2, and 4^1E states corresponds to $CH_3\ (3p\ ^2E) + F\ (^2P)$. Corresponding dissociation energies will be discussed later.

The ionic complex and its dissociation behavior were investigated in more detail using a CAS(6,4) reference wave function including only valence orbitals and using the aug-cc-pVDZ and aug′-cc-pVTZ basis sets. Figure 4 shows the dissociation curves obtained for states 1^1A_1, 1^1E, and 2^1A_1. The effect of the basis set on the shape of the potential curves is relatively small. For this reason, only the potential curves obtained by using aug′-cc-pVTZ were presented. The correct dissociation profile is obtained as orbitals $5a_1$ and $6a_1$ smoothly change from σ_{CF} and σ^*_{CF} character to $F(p_{a1})$ and $C(p_{a1})$ atomic orbitals, leading at larger CF distances to the dominant configurations $F(p_{a1})^1C(p_{a1})^1$ in the ground-state dissociation limit and $F(p_{a1})^2C(p_{a1})^0$ in the ionic $F^-(^1S) + CH_3^+\ (^1A_1)$ case, respectively. The ground-state minimum obtained at the CASSCF level is found at a C−F distance that is 0.28 Å larger than those computed with post-CASSCF methods. The CASSCF

TABLE 2: Dissociation Energies (eV) for $CH_3F \rightarrow CH_3 + F$ Relative to the Ground State Computed with Different Approaches at the MR-CISD and MR-CISD+Q Levels Using the d-aug′-cc-pVDZ Basis Set in Comparison with Experimental Reference Values

		case I[a]		case II		case III[b]		exptl reference
state	dissociation limit	CISD	CI+Q	CISD	CI+Q	CISD	CI+Q	values
1^1A_1, 1^1E	$CH_3(\tilde{X}\ ^2A_2'') + F(^2P)$	5.08	4.83	5.08	4.83	4.77	5.14	5.05
2^1E, 2^1A_1	$CH_3(3s\ ^2A_1') + F(^2P)$	10.60	10.55	10.83	10.74	11.30	11.80	10.79
3^1A_1	$CH_3^+(\tilde{X}^1A_1') + F^-(^1S)$	12.22	11.29	11.83	11.34	12.66	12.64	11.44
3^1E, 1^1A_2, 4^1E, 4^1A_1	$CH_3(3p\ ^2A_2'') + F(^2P)$	11.84	11.82	12.14	12.09	12.50	13.09	12.54

[a] Total energies (hartrees) in the order of dissociation limits given in the Table: MR-CISD −139.237751; −139.034637; −138.975434; −138.989251, MR-CISD+Q −139.267464; −139.057030; −139.030049; −139.010517. Ground-state energies: −139.424344 (MR-CISD) and −139.444891 (MR-CISD+Q). [b] Total energies (hartrees) in the order of dissociation limits given in the Table: MR-CISD −139.227043; −138.987049; −138.937100; −138.943238, MR-CISD+Q −139.257460; −139.012660; −138.981679; −138.965341. Ground-state energies are given in Table 1.

ground-state dissociation energy is significantly lower by 1.9−2.3 eV than those obtained with the other methods used in this work. The ordering among calculated dissociation curves and energies for the 1^1A_1 and 1^1E states is CASSCF < MR-CISD < MR-CISD+Q. For the 2^1A_1 state, the inverse situation is observed. The MR-CISD+Q curve is the lowest one. The reason for this behavior is that for the proper description of F^- in the ionic structure a more extended representation of dynamical electron correlation relative to the ground state is required. A comparison of the results obtained at the MR-CISD and MR-CISD+Q levels using aug-cc-pVDZ and aug′-cc-pVTZ will be discussed in detail in the following sections.

The ionic complex ($CH_3^+F^-$) in the 2^1A_1 state is a minimum under C_{3v} symmetry restrictions. Geometry optimization at the MR-CISD level using the CAS(6,4) reference space and the aug′-cc-pVTZ basis of this minimum led to a structure with $R_{CF} = 2.77$ Å and a planar substructure of the CH_3 fragment ($\angle_{H''H''} = 120°$ and $\angle_{FCH'} = 88.1°$). The angle of 88.1° indicates a small deviation from the C_{3v} structure. Nevertheless, this structure will be referenced under this symmetry label in the text below. A vibrational analysis carried out at the SA-CASSCF level showed that this structure corresponded to a second-order saddle point. The analysis of the imaginary frequencies suggested distortions to C_s symmetry. This point will be discussed below.

C. Dissociation Energies. The experimental enthalpy difference for the gas-phase $CH_3F \rightarrow CH_3 + F$ dissociation is 4.76 eV.[36] To compare this experimental value with our calculated energy differences, zero-point energy corrections computed at the SA-MCSCF level were applied to the experimental enthalpy difference. The zero-point energies obtained for the CH_3F molecule and the $CH_3 + F$ supermolecule were 9013.0 and 6696.1 cm^{-1}, respectively, leading to 5.05 eV for the experimental dissociation energy of CH_3F in the ground state. The experimental, adiabatic excitation energies of the CH_3 radical have been reported as 5.74 eV ($\tilde{X}^2A_2'' \rightarrow 3s\ ^2A_1'$)[37] and 7.45 eV ($\tilde{X}^2A_2'' \rightarrow 3p\ ^2A_2''$).[38] Again, these values were corrected by zero-point energy differences. The zero-point energies calculated at the MCSCF level for CH_3 ($\tilde{X}^2A_2''$), CH_3 ($3s\ ^2A_1'$), and CH_3 ($3p\ ^2A_2''$) are 6984.2, 6947.4, and 6656.1 cm^{-1}, respectively. Corresponding zero-point energy corrections are −0.005 eV (for $\tilde{X}\ ^2A_2'' \rightarrow 3s\ ^2A_1'$) and −0.04 eV (for $\tilde{X}\ ^2A_2'' \rightarrow 3p\ ^2A_2''$). Taking these values into consideration, we report zero-point-energy-corrected adiabatic experimental excitation energies of 5.74 and 7.49 eV. Combining the corrected experimental value for the dissociation energy (5.05 eV) and the just-mentioned corrected adiabatic excitation energies for CH_3, we find the experimental reference values for the dissociation energy of channels CH_3 ($3s\ ^2A_1'$) + $F(^2P)$ and CH_3 ($3p\ ^2A_2''$) + $F(^2P)$ with respect to the ground-state energy to be 10.79 and 12.54 eV, respectively. The reference value for the dissociation energy of the ionic channel has been obtained as the sum of the corrected experimental ground-state dissociation energy, the experimental values for the electron affinity of fluorine (3.40 eV),[39] and the ionization energy of the methyl radical (9.84 eV),[40] corrected by the calculated zero-point energy differences obtained at the MCSCF level for CH_3 and CH_3^+ (0.01 eV). The resulting dissociation level is located 11.44 eV above the CH_3F ground-state minimum. These experimental reference values are collected in Table 2.

TABLE 3: Vertical and Adiabatic Excitation Energies for CH_3, Ionization Energy of CH_3, and Electron Affinity of Fluorine[a−c]

		CISD	CI+Q	exptl
$CH_3\ (\tilde{X}\ ^2A_2'') \rightarrow CH_3\ (3s\ ^2A_1')$	vertical	5.66	5.81	
	adiabatic	5.75	5.91	5.74[d]
$CH_3\ (\tilde{X}\ ^2A_2'') \rightarrow CH_3\ (3p\ ^2A''_2)$	vertical	6.90	7.07	
	adiabatic	7.02	7.22	7.45[e]
CH_3 ionization energy	vertical	9.53	9.68	9.84[f]
	adiabatic	9.51	9.66	
F electron affinity		2.75	3.14	3.40[g]

[a] Energy differences in eV. [b] Total ground-state energies (hartrees): CH_3: MR-CISD −39.711393, MR-CISD+Q −39.725102; fluorine: MR-CISD −99.535419, MR-CISD+Q −99.544755. [c] Optimized CH distance for CH_3 (D_{3h} symmetry) at the MCSCF level: $\tilde{X}\ ^2A_2''$ 1.074 Å, $3s\ ^2A_1$ 1.095 Å, $3p\ ^2A_2''$ 1.085 Å. Optimized CH distance for CH_3^+ ($\tilde{X}\ ^1A_1'$) at the MCSCF level: 1.096 Å. [d] Reference 37. [e] Reference 38. [f] Reference 40. [g] Reference 39.

Ground-state dissociation energies of 5.08 and 4.83 eV (MR-CISD and MR-CISD+Q) were obtained in calculations according to case I (Table 2). A relatively large quadruple correction of 0.25 eV to the MR-CISD energy is observed. The MR-CISD+Q value is 0.22 eV smaller than the experimental reference value, a difference that is quite acceptable within the limits of our approaches. The ground-state dissociation energies taken from the potential energy curves (case III) are 4.77 and 5.14 eV at the MR-CISD and MR-CISD+Q levels, respectively.

The vertical excitation energies to the $3s\ ^2A_1'$ state of CH_3 are 5.66 and 5.81 eV at the MR-CISD and MR-CISD+Q levels, respectively (Table 3). Corresponding adiabatic excitation energies are 5.75 and 5.91 eV. These results are quite close to the experimental value of 5.74 eV.[37] The adiabatic excitation energies to the $3p\ ^2A_2''$ state at the MR-CISD and MR-CISD+Q levels are 7.02 and 7.22 eV, in quite good agreement with the experimental value of 7.45 eV.[38] The adiabatic ionization energy of 9.66 eV for CH_3 at the MR-CISD+Q level compares well with the experimental value of 9.84 eV.[40] Values of 2.75 and 3.14 eV were found for the fluorine electron affinity at the MR-CISD and MR-CISD+Q levels, respectively, in reasonable agreement with the literature value of 3.40 eV.[39] Taking the

TABLE 4: Optimized Geometries (Bond Distances in Å, Angles in Degrees) and Total Energies (in hartrees) for $CH_3F(1^1A')$, $CH_3^+F^-(3^1A')$, $H_2CHF(3^1A')$, and FH_2CH $(3^1A')$ at the MR-CISD/CAS(6,4) Level

$CH_3F(1^1A')$

	CF	CH	HCH	FCH	energy[a]
aug-cc-pVDZ	1.363	1.102	109.4	109.5	−139.398381 (−139.439698)
aug′-cc-pVTZ	1.338	1.092	108.8	110.1	−139.505171 (−139.550872)

$CH_3^+F^-(3^1A')$

	CF	CH	HCH	FCH	energy[a]
aug-cc-pVDZ	2.797	1.089	120.0	88.1	−139.144200 (−139.197990)
aug′-cc-pVTZ	2.770	1.076	120.0	88.1	−139.241277 (−139.300737)

$H_2CHF(3^1A')$[b]

	CF	CH′	CH″	H″CH″	H′CH″	FCH′	energy[a]
aug-cc-pVDZ	2.684	1.160	1.093	116.1	122.0	0.0	−139.189882 −139.241644
aug′-cc-pVTZ	2.646	1.155	1.079	116.1	121.9	0.0	−139.287264 (−139.345043)

$FH_2CH(3^1A')$[b]

	CF	CH′	CH″	H″CH″	H′CH″	FCH′	energy[a]
aug-cc-pVDZ	2.501	1.092	1.094	111.1	124.5	180.0	−139.173525 (−139.229204)
aug′-cc-pVTZ	2.475	1.079	1.081	111.0	124.5	180.0	−139.270759 (−139.332306)

[a] MR-CISD+Q energies are shown in parentheses. [b] For the definition of geometrical parameters, see Figure 1.

calculated adiabatic excitation/ionization energies (including zero-point energy differences) as well as the fluorine electron affinity along with the ground-state dissociation energy obtained for case I into account, we find the dissociation energies for CH_3 ($3s\ ^2A_1'$) + $F(^2P)$, $CH_3^+(\tilde{X}^1A_1')$ + $F^-(^1S)$, and CH_3 ($3p\ ^2A_2''$) + $F(^2P)$ to be 10.74, 11.34, and 12.09 eV, respectively, at the MR-CISD+Q level (Table 2, case II).

Dissociation energies for the excited states according to cases I−III are summarized in Table 2. The agreement of adiabatic values (case II) with experimental reference values is quite good. Total errors are composed of the common error in the ground-state dissociation energy and individual errors for the different excitation and ionization energies of CH_3 and the electron affinity of F. A comparison with case III results gives information on geometry relaxation effects with respect to the dissociation using the frozen CH_3 geometry. This effect is most pronounced for the dissociation to the $3p\ ^2A_2''$ state of CH_3 and for the ionic state. In total, one can conclude from this comparison that the fixed-geometry dissociation curves presented in Figures 2 and 3 give a reliable overview. If one wants to obtain more accurate results, geometry relaxation effects are important. These effects have been taken into account at finite C−F bond distances only for the ionic state in order to locate the global energy minimum.

D. Bent Structures. FCH′ bending curves were calculated for the first four electronic states $1^1A'$, $2^1A'$, $1^1A''$, and $3^1A'$ at the MR-CISD level on the basis of a CAS(12,7) reference wave function and the aug-cc-pVDZ basis set. These curves were calculated under C_s symmetry restrictions with the symmetry plane bisecting the CH''_2 group and containing the F atom (Figure 1) starting from the optimized 2^1A_1 state for the ionic $CH_3^+F^-$ complex. The bending curves indicated two stationary points for the $3^1A'$ state with FCH′ angles around 0 and 180°.

In the next step, geometry optimizations under C_s symmetry restrictions were performed for these structures in the $3^1A'$ state at the MCSCF and MR-CISD levels using the CAS(6,4) reference space and the aug-cc-pVDZ and aug′-cc-pVTZ basis sets. These optimizations gave two structures: H_2CHF with $\angle_{FCH'} = 0°$ and FH_2CH with $\angle_{FCH'} = 180°$. Optimized geometries are shown in Table 4. For comparison, the optimized geometries of CH_3F ($1^1A'$ state) and $CH_3^+F^-$ ($3^1A'$ state) are given in Table 4 also. The dominant configurations in the CASSCF and MR-CISD wave functions show that these structures correspond to ionic complexes. The C−F distance in H_2CHF ($3^1A'$) is about 1.30 Å longer than in CH_3F ($1^1A'$), and the C−H′ bond is significantly stretched by 0.06 Å. For FH_2CH ($3^1A'$), the MR-CISD calculations show that the hydrogen atoms are attached to the carbon atom with standard C−H distances lying in the range of 1.076−1.092 Å. The change from the aug-cc-pVDZ to the aug′-cc-pVTZ basis set led to a decrease in the C−F distances for these structures by 0.03−0.04 Å, and the C−H distances were shortened by 0.01 Å. No significant variation was found for the angles with the change in the basis set. Computed vibrational frequencies show that the H_2CHF ($3^1A'$) structure is a local minimum, whereas FH_2CH ($3^1A'$) is a saddle point. The imaginary vibrational mode corresponds to the in-plane angular movement of the fluorine atom along the FCH′ angle. The energy barriers are 0.45 and 0.34 eV at the MR-CISD and MR-CISD+Q levels, respectively.

Starting from the optimized $H_2CHF(3^1A')$ structure at the MR-CISD level using the CAS(6,4) reference space and the aug′-cc-pVDZ basis set, we computed a potential energy curve in the C−F distance by fixing the C−F distance and reoptimizing all of the other internal coordinates. Results are shown in Figure 5. From this figure, an avoided crossing between the $1^1A'$ and $3^1A'$ states near 2.8 Å is observed. At C−F distances smaller than 2.8 Å, state $1^1A'$ corresponds to the ionic $CH_3^+F^-$ state, and $3^1A'$ corresponds to the covalent $F-CH_3$ state. At about 2.8 Å, these configurations interchange, leading to dissociation into $F(^2P)$ + $CH_3(\tilde{X}^2A_2'')$ for the $1^1A'$, $2^1A'$, and

TABLE 5: Dissociation Energies (eV) for $CH_3F(1^1A_1)$, $CH_3^+F^-(3^1A')$, $H_2CHF(3^1A')$, and FH_2CH $(3^1A')$ at the MR-CISD and MR-CISD+Q Levels Using Different Basis Sets[a]

		MR-CISD	MR-CISD+Q
$CH_3F(1^1A_1) \rightarrow CH_3(\tilde{X}\ ^2A_2'') + F(^2P)$	aug-cc-pVDZ	4.27	4.68
	aug′-cc-pVTZ	4.36	4.73
$CH_3F(1^1A_1) \rightarrow CH_3^+(\tilde{X}^1A_1') + F^-(^1S)$	aug-cc-pVDZ	11.45	10.99
	aug′-cc-pVTZ	11.74	11.26
$CH_3^+F^-(3^1A') \rightarrow CH_3^+(\tilde{X}^1A_1') + F^-(^1S)$	aug-cc-pVDZ	4.53	4.41
	aug′-cc-pVTZ	4.56	4.46
$H_2CHF(3^1A') \rightarrow CH_3^+(\tilde{X}^1A_1') + F^-(^1S)$	aug-cc-pVDZ	5.77	5.60
	aug′-cc-pVTZ	5.82	5.67
$FH_2CH(3^1A') \rightarrow CH_3^+(\tilde{X}^1A_1') + F^-(^1S)$	aug-cc-pVDZ	5.33	5.26
	aug′-cc-pVTZ	5.37	5.32

[a] For all calculations, the CAS(6,4) reference space was used.

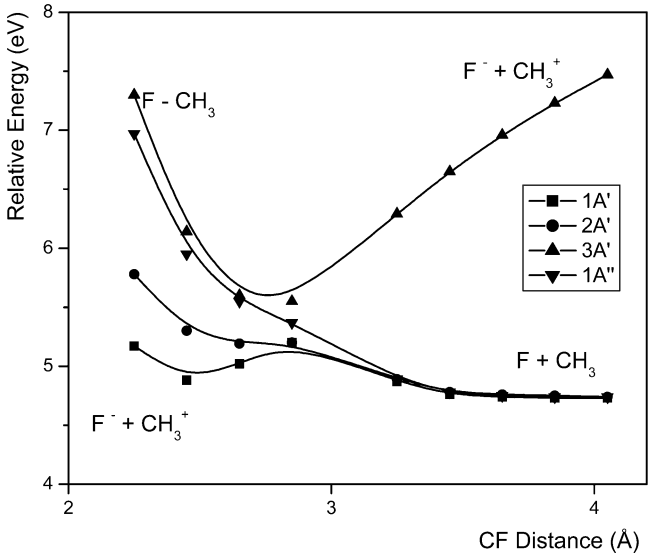

Figure 5. Dissociation curves for H_2CHF at the MR-CISD level using a CAS(6,4) reference space and the aug′-cc-pVTZ basis set.

$1^1A''$ states and to $F^-(^1S) + CH_3^+(\tilde{X}\ ^1A_1')$ in the case of state $3^1A'$. States $1^1A'$ and $3^1A'$ are correlated (at the dissociation limit) to the 1^1A_1 and 3^1A_1 states, respectively, of Figure 1. States $2^1A'$ and $1^1A''$ are degenerate in this case and correspond to the 1^1E state.

Dissociation energies were calculated for the stationary points of all ionic structures by computing the energy difference of the optimized structures with respect to the optimized supermolecule with a C−F distance of 50 Å and corrected by the remaining Coulomb energy. For the results, see Table 5. The dissociation energy of the $3^1A'$ H_2CHF structure with respect to the ionic dissociation limit $CH_3^+(\tilde{X}^1A_1) + F^-(^1S)$ is 5.82 eV at the MR-CISD level and 5.67 eV at the MR-CISD+Q level (aug′-cc-pVTZ basis). Thus, this structure is more stable than the C_{3v} structure (MR-CISD+Q dissociation energy 4.46 kcal/mol) by 1.2 eV. A comparison between dissociation energies obtained with the aug-cc-pVDZ and aug′-cc-pVTZ results shows that the larger basis set causes the dissociation energies to increase only by 0.03−0.07 eV. Thus, the smaller aug-cc-pVDZ describes the energetics of the dissociation processes of the ionic species very well. A similar conclusion could be made above when comparing the dissociation curves for the C_{3v} structure.

V. Conclusions

Calculated vertical excitation energies are in good agreement with experimental data. Assignments for the observed peaks in the experimental spectra were reanalyzed, and our results mostly confirm the experimental assignments but suggest some modifications for the main contribution to the maximum observed in the range from 12.5−14 eV. From computed oscillator strengths, we conclude that the main contribution to this band comes from the $\sigma_{CF} \rightarrow 3p_{a1}$ excitation rather than from the $\sigma_{CF} \rightarrow 3s$ excitation.

The dissociation channels for the production of fluorine atoms have been characterized. The computed energy curves show that the vertically excited states are connected in all cases except for one through repulsive curves to the dissociation limits characterized by the fluorine atom in the ^2P ground state and by CH_3 in the ground state and the first two excited states. A fluoride-formation path (an ionic channel suggested in plasma chemical kinetic models[4,5]) has also been found, which proceeds via a minimum-energy structure. This minimum structure is of the form H_2CHF and is strongly bound by 5.67 eV with respect to the ionic dissociation limit of $F^- + CH_3^+$.

Acknowledgment. We acknowledge support by the Austrian Science Fund within the framework of Special Research Program F16 and Project P1442-CHE. G.F.B. thanks the CNPq, Brazil, for financial support. The calculations were performed in part on the Schrödinger II Linux Clusters of the Vienna University Computer Center.

References and Notes

(1) Jung, C. O.; Chi, K. K.; Hwang, B. G.; Moon, J. T.; Lee, M. Y.; Lee, J. G. *Thin Solid Films* **1999**, *341*, 112.
(2) Balachova, O. V.; Alves, M. A. R.; Stwart, J. W.; Braga, E. S.; Cescato, L. *Microelectron. J.* **2000**, *31*, 213.
(3) Heber, G. A. *Appl. Surf. Sci.* **2002**, *192*, 161.
(4) Bauerfeldt, G. F.; Arbilla, G. *J. Braz. Chem. Soc.* **2000**, *11*, 121.
(5) Bauerfeldt, G. F.; Arbilla, G. *J. Braz. Chem. Soc.* **2000**, *11*, 129.
(6) Jalbout, A. F. *J. Mol. Struct.: THEOCHEM* **2002**, *618*, 35.
(7) Espinosa-Garcia, J. *Chem. Phys. Lett.* **1996**, *250*, 71.
(8) NcGivern, W. S.; Derecskei-Kovacs, A.; North, S. W.; Francisco, J. S. *J. Phys. Chem. A* **2000**, *104*, 436.
(9) Duncan, J. L. *J. Mol. Struct.* **1970**, *6*, 447.
(10) Egawa, T.; Yamamoto, S.; Nakata, M.; Kuchitsu, K. *J. Mol. Struct.* **1987**, *156*, 213.
(11) Demaison, J.; Breidung, J.; Thiel, W.; Papoušek, D. *Struct. Chem.* **1999**, *10*, 129.
(12) Locht, R.; Leyl, B.; Hoxha, A.; Dehareng, D.; Jochims, H. W.; Baumgärtel, H. *Chem. Phys.* **2000**, *257*, 283.
(13) Shavitt, I. In *Methods of Electronic Structure Theory*; Schaefer, H. F., III, Ed.; Plenum: New York, 1977.
(14) Shepard, R.; Lischka, H.; Szalay, P. G.; Kovar, T.; Ernzerhof, M. *J. Chem. Phys.* **1991**, *93*, 2085.
(15) Shepard, R. In *Modern Electronic Structure Theory*, part I; Yarkony, D. R., Ed.; World Scientific: Singapore, 1995.
(16) Lischka, H.; Dallos, M.; Shepard, R. *Mol. Phys.* **2002**, *100*, 1647.
(17) Langhoff, S. R.; Davidson, E. R. *Int. J. Quantum Chem.* **1974**, *8*, 61.
(18) Bruna, P. J.; Peyerimhoff, S. D.; Buenker, R. J. *Chem. Phys. Lett.* **1981**, *72*, 278.
(19) Müller, Th.; Lischka, H. *Theor. Chem. Acc.* **2001**, *106*, 369.
(20) Dallos, M.; Lischka, H. *Theor. Chem. Acc.*, in press.
(21) Dunning, T. H., Jr. *J. Chem. Phys.* **1989**, *90*, 1007.

(22) Kendall, R. A., Dunning, T. H., Jr., Harrison, R. J. *J. Chem. Phys.* **1992**, *96*, 6796.
(23) Woon, D. E.; Dunning, T. H., Jr. *J. Chem. Phys*. **1994**, *100*, 2975.
(24) van Mourik, T.; Wilson, A. K.; Dunning, T. H., Jr. *Mol. Phys.* **1999**, *96*, 529.
(25) Bunge. A. *J. Chem. Phys.* **1970**, *53*, 20.
(26) Lischka, H.; Shepard, R.; Brown, F. B.; Shavitt, I. *Int. J. Quantum Chem. Quantum Chem. Symp.* **1981**, *15*, 91.
(27) Shepard, R.; Shavitt, I.; Pitzer, R. M.; Comeau, D. C.; Pepper, M.; Lischka, H.; Szalay, P. G.; Ahlrichs, R.; Brown, F. B.; Zhao, J. *Int. J. Quantum Chem. Quantum Chem. Symp.* **1988**, *22*, 149.
(28) Lischka, H.; Shepard, R.; Pitzer, R. M.; Shavitt, I.; Dallos, M.; Müller, Th.; Szalay, P. G.; Seth, M.; Kedziora, G. S.; Yabushita, S.; Zhang, Z. *Phys. Chem. Chem. Phys.* **2001**, *3*, 664.
(29) Lischka, H.; Shepard, R.; Shavitt, I.; Pitzer, R. M.; Dallos, M.; Müller, Th.; Szalay, P. G.; Brown, F. B.; Ahlrichs, R.; Böhm, H. J.; Chang, A.; Comeau, D. C.; Gdanitz, R.; Dachsel, H.; Erhard, C.; Ernzerhof, M.; Höchtl, P.; Irle, S.; Kedziora, G.; Kovar, T.; Parasuk, V.; Pepper, M.; Scharf, P.; Schiffer, H.; Schindler, M.; Schüller, M.; Zhao, J.-G. *COLUMBUS: An Ab Initio Electronic Structure Program*, release 5.9; 2003.
(30) Helgaker, T.; Jensen, H. A.; Jørgensen, P.; Olsen, J.; Ruund, K.; Agren, H.; Andersen, T.; Bak, K. L.; Bakken, V.; Christiansen, O.; Dahle, P.; Dalskov, E. K.; Enevoldsen, T.; Heiberg, H.; Hettema, H.; Jonsson, D.; Kirpekar, S.; Kobayashi, R.; Koch, H.; Mikkelsen, K. V.; Norman, P.; Packer, M. J.; Saue, T.; Taylor, P. K.; Vahtras, O. *DALTON: An Ab Initio Electronic Structure Program*, release 1.0; 1997.
(31) Fogarasi, G.; Zhou, X.; Taylor, P. W.; Pulay, P. *J. Am. Chem. Soc.* **1992**, *114*, 8191.
(32) Csaszar, P.; Pulay, P. *J. Mol. Struct.* **1984**, *114*, 31.
(33) Pulay, P.; Fogarasi, G.; Pongor, G.; Boggs, J. E.; Vargha, A. *J. Am. Chem. Soc.* **1983**, *105*, 7037.
(34) Olney, T. N.; Cooper, G.; Chan, W. F.; Burton, G. R.; Brion, C. E.; Tan, K. H. *Chem. Phys.* **1994**, *189*, 733.
(35) Harshbarger, W. R.; Robin, M. B.; Lassettre, E. N. *J. Electron. Spectrosc. Relat. Phenom.* **1973**, *1*, 319.
(36) Chase, M. W., Jr. *J. Phys. Chem. Ref. Data* **1998**, Monograph 9, 1−1951.
(37) Westre, S. G.; Gansberg, T. E.; Kelly, P. B.; Ziegler, L. D. *J. Chem. Phys.* **1992**, *96*, 3610.
(38) Hudgens, J. W.; DiGiuseppe, T. D.; Lin, M. C. *J. Chem. Phys.* **1973**, *79*, 571.
(39) Blondel, C.; Delsart, C.; Goldfarb, F. *J. Phys. B: At. Mol. Opt. Phys.* **2001**, *34*, L281.
(40) Houle, F. A.; Beauchamp, J. L. *J. Am. Chem. Soc.* **1979**, *101*, 4067.